



**POLITECNICO**  
MILANO 1863

SCUOLA DI INGEGNERIA INDUSTRIALE  
E DELL'INFORMAZIONE

EXECUTIVE SUMMARY OF THE THESIS

## De-orbiting mission from LEO: design of a passive deployment system for an origami drag sail

LAUREA MAGISTRALE IN SPACE ENGINEERING - INGEGNERIA SPAZIALE

**Author:** TOMMASO SIRONI

**Advisor:** PROF. ANTONIO MATTIA GRANDE

**Co-advisor:** LAURA PERNIGONI

**Academic year:** 2021-2022

### 1. Introduction

Many of the subsystems equipping space vehicles are made up of structures requiring large dimensions to provide performance compatible with the mission requirements. The research about these systems mainly concerns the minimization of packed volume and the deployment strategy. As regards the first, interest in origami's application in space engineering has grown in the last years since they reduce the space filled up by the membrane structures inside the satellite and guarantee simple and effective deployment. Secondly, the deployment actuators are nowadays driven by electric motors or elastic force release and the research is oriented toward the use of passive actuation systems. In this context, shape memory materials respond to the requirement of a passive and compact actuation system. In the following lines, the deployment of a large origami membrane structure with the aid of SMA wires is investigated. The case study is a drag sail for LEO de-orbiting.

### 2. Case study

The design of the de-orbiting system (dimensions and actuation device) refers to a 3U Cube-

Sat (mass of about 4kg) orbiting in LEO at an altitude of 750km. These choices are based on the recent need to reduce the overcrowding of space debris in LEO and the increase in the number of small satellites launched every year. The sail is made of a Kapton structural film coated with thin aluminum layers for an overall thickness of  $10\mu\text{m}$ , consistent with the literature.

### 3. De-orbiting design

#### 3.1. De-orbit model

The design of the actuation system is carried out after sizing the drag sail membrane structure. The satellite orbiting in LEO must reenter the atmosphere within five years after the end of its operational life, as ruled by the FCC. For this purpose, the restricted two-body problem [2] is implemented in MATLAB® to predict the minimum dimension of the sail required to de-orbit within the lifetime limit (equation 1).

$$\ddot{\mathbf{r}} = -\frac{\mu}{r^3}\mathbf{r} + \sum \mathbf{a}_p. \quad (1)$$

The term  $\sum \mathbf{a}_p$  indicates the perturbing acceleration involved in the design. The first is the solar radiation pressure, which is assumed constant with the orbital altitude and varies with

the attitude of the satellite. The acceleration due to air drag is the main contribution to the de-orbiting and it is modeled with the aid of COSPAR International Reference Atmosphere model from NSSDC. Lastly, the Earth’s zonal harmonics are implemented to model its uneven distribution of mass. The first two accelerations are exploited by the sail for de-orbiting purposes, while zonal harmonics act as perturbations.

Since the magnitude and direction of the accelerations depend on the attitude of the satellite, it must orient in such a way the deceleration is maximized. Above 1000km, where the density of the atmosphere is null, the sail exploits the SRP only. When the spacecraft moves towards the Sun the attitude aims at maximizing the cross-sectional area impinged by the photons, while the area is minimized when the photons would contribute to accelerating the satellite. On the other hand, when the altitude drops down to the point where air pressure overcomes the SRP, the cross-sectional area is maximized with respect to the acceleration due to air drag. This second strategy guarantees an effective de-orbit for satellites orbiting in LEO.

The above de-orbit model allows finding the minimum dimension of the sail capable of making the satellite reenter into the atmosphere within 5 years. Each altitude is associated with a sail size meeting this lifetime requirement, as shown in Figure 1, which is equivalent to  $1.04\text{m}^2$  for a starting orbit of 750km. An area of  $1.5\text{m}^2$  will be considered to account for the high variability of the de-orbit lifetime and the inaccuracy of the model.

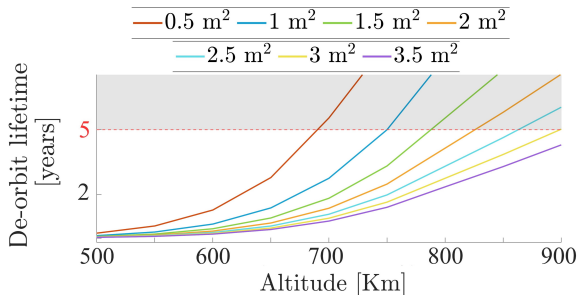


Figure 1: De-orbit lifetime.

### 3.2. Model validation

The result is validated with the aid of Ansys STK Premium Space software, an advanced analytical tool providing a time-dynamic modeling

environment to model complex systems inside a realistic and three-dimensional simulation. Although its accuracy is not better than 10% of the actual lifetime, it is valid to prove the reliability of the result. Therefore, the size of the sail obtained from STK is  $1.01\text{m}^2$  and demonstrates the effectiveness of the implemented model. It is interesting to notice the growth in the difference between the two results as the starting orbital altitude increases. The reason may lie in the accuracy of the atmospheric model at high altitudes.

### 3.3. Optimized origami pattern

The dimension of the sail is the input to the origami optimization software [3], which provides the main characteristics of the origami sail: number of cells along the two directions, face sides length and angles, packed volumes, and overall mass. The selected origami pattern is the Miura-Ori, because of its high  $A_{deployed}/V_{packed}$  ratio, its simple deployment kinematics, and its homogeneity in deployed size. By setting the volume of a 1U (10cmx10cmx10cm) as the maximum packed dimension, the result is a sail perfectly fitting inside that volume and having the required deployed size, as reported in table 1.

Optimized drag sail module	
Side $a$ length [m]	0.028
Side $b$ length [m]	0.016
Total deployed surface [ $\text{m}^2$ ]	1.52
Percentage of occupied volume (1U)	5.2%
Number of cells in X direction	20
Number of cells in Y direction	11

Table 1: Optimized origami drag sail.

## 4. Thermal analysis

### 4.1. Thermal model

The actuation system for the deployment of the drag sail is based on the shape memory effect occurring as a consequence of the temperature-induced transformation of SMA. The thermal analysis of the de-orbiting system is thus crucial to verify whether the actuation of shape memory material can be achieved without resorting to Joule effect heating. The implemented heat transfer model focuses on the flow of thermal energy that takes place between the sail and the

external environment, according to the first law of thermodynamics. A single-node lumped parameter approach is carried out, meaning that the sail is modeled as a single body with a homogeneous temperature. Considering the density  $\rho$  of the system constant, no work exchange, and no internal heat sources, the heat transfer formulation assumes the expression:

$$\rho V c_V \frac{\partial T}{\partial \tau} = \sum \dot{Q}. \quad (2)$$

$\sum \dot{Q}$  in equation 2 is the summation of all the heat rate involved. The main one is due to the radiation coming from the Sun,  $\dot{Q}_{Sun}$ . The Earth provides its contribution too, both by infrared radiation  $\dot{Q}_{IR}$  and reflection of the Sun's radiation  $\dot{Q}_{alb}$ , but it is less effective than  $\dot{Q}_{Sun}$ . Besides the incoming radiation, the space objects emit toward deep space,  $\dot{Q}_{ds}$ , balancing the heat exchange. A last relevant contribution is the aerodynamic heating due to the high-speed interaction with the upper rarefied layers of the atmosphere.  $\dot{Q}_{air-drag}$  depends on the density of the atmosphere and thus it is almost null over the entire de-orbiting. However, when the altitude drops below 150km, the value increases sharply and is responsible for the satellite burning. On the one hand, this analysis is interesting for identifying the thermal cycles to which the sail is subjected. On the other, the focus is on the deployment phase, so the heat transfer formulation must be deepened accounting for the radiation among the origami faces.

#### 4.2. Monte Carlo method

When the sail is even only partially folded, the heat exchanged becomes a function not only of the attitude but also of the deployment angle because of the self-radiation and reflection of neighboring faces. Therefore, it is necessary to compute a self-view factor evaluating the amount of radiation exchanged with the sail itself. The first method to compute the self-view factor is based on the analytical integration of the view factor among differential surfaces. This solution is laborious because of the high number of faces radiating from each other, so the Monte Carlo simulation is preferred, a computational algorithm used to model the probability of a certain outcome with the random generation of samples. Figure 2 provides an idea of the procedure adopted.

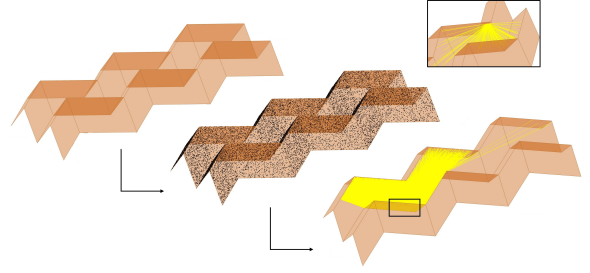


Figure 2: Monte Carlo method for the computation of the Miura-Ori self-view factor.

The first step consists of the random generation of points on the three-dimensional origami model faces. A specified number of randomly directed rays is then driven out of the faces starting from the previously generated points and they are selected based on whether they spread out into the surrounding space or they hit the sail itself. The latter rays define the self-view factor of the Miura-Ori, which can be computed for any folding angle. It is important to notice that the value just obtained depends on the face from which the rays are shot, since in the faces close to the perimeter of the sail the self-view factor is less than the innermost one. However, the high number of cells making up the membrane justifies the choice of adopting the single-node approach, and the self-view factor is computed as a weighted average of the self-view factors of each face of the Miura-Ori. More detailed modeling should investigate a multi-node parameter approach.

#### 5. Multi-body dynamics model

The geometric and thermal designs of the sail are preparatory to the deployment simulation model of the system. Since the target is to verify the effectiveness of the passive actuator, the dynamic model is suitable to involve the forces inducing the deployment of the membrane structure. In particular, this work focuses on multi-body dynamics simulation, modeling each face of the origami pattern as a rigid body connected with the neighboring ones through joints. The system is described by Lagrange's equations of motion plus a set of kinematic constraints:

$$\mathbf{M}\ddot{\mathbf{q}} + \mathbf{f}_D + \Phi_q^T \lambda - \mathbf{Q} = 0 \quad (3)$$

$$\Phi(\mathbf{q}, t) = 0 \quad (4)$$

with  $\mathbf{q}$  representing the vector of generalized

nodal coordinates of the bodies that make up the system. The strength of the dynamic analysis is the ability to model complex systems ensuring low computational efforts with respect to finite element analysis. Moreover, even if thin membrane structures are provided with high flexibility, this modeling guarantees results in line with the real behavior of the structure.

Among the software designed for the simulation of complex multibody systems, ADAMS is the best and most widely used. A big advantage of ADAMS is the ability to integrate simulation and modeling with MATLAB, simplifying both the design and the analysis of the results [4]. Therefore, the scheme in figure 3 is the one followed from the preliminary design up to the complete simulation.

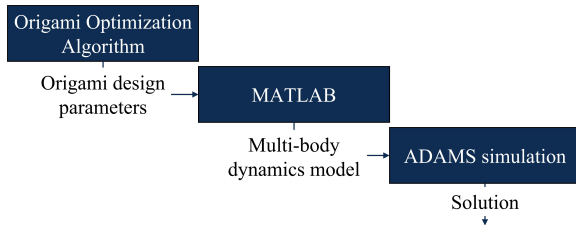


Figure 3: Sail dynamics analysis: block scheme.

The optimized parameters of the origami are imported into a MATLAB code generating the *.OBJ* file to be sent to ADAMS and collecting the information about the geometry of the origami. Each body is assigned its physical and mechanical properties (density, Young’s modulus, Poisson’s ratio), and the mass and the inertia are automatically generated in the software. At this point, a set of independent elements is generated, which requires the definition of the joints. The crease lines can be modeled as simple revolute joints enabling the rotation about the joint axis. Even if they faithfully represent the relative movement of the faces, simulation issues can arise because of the high number of redundant constraints. Two are the solutions to this problem. First, a degrees-of-freedom analysis leads to a more accurate definition of the joints, comprising both spherical type and cylindrical in addition to revolute. A second strategy involves the bushing forces, joint-like elements with three translational and three rotational degrees of freedom, each of them associated with a stiffness value. By setting the stiffness of the not-allowed degrees of freedom to very high val-

ues and the one of the rotation along the crease line as zero, the result is an equivalent revolute joint not causing simulation issues.

However, contrary to what is stated above, the stiffness of the revolute joint is not null since the plastic deformation of the crease opposes the recovery of the original flat shape. The folding lines are thus modeled as equivalent torsional springs whose stiffness depends on the sail thickness and crease length. The moment opposed is:

$$M = kW(\theta - \phi) \quad (5)$$

with a value of  $k = 0.0001\text{N}\cdot\text{deg}^{-1}$  for  $25\mu\text{m}$  thick Kapton films, found experimentally. More accurate crease stiffness models can be investigated in future works. The damping effect associated with the stiffness is computed as  $c = 2\zeta\sqrt{KI}$ , in which the damping ratio is about 0.5. More precise values for  $\zeta$  can be obtained through future experimentation, e.g., by using the logarithmic decrement method.

Finally, the rigid translations and rotation of the deploying structure must be constrained. The most used strategy is to ground one of the faces of the origami, granting the deployment of the others around it.

## 6. Passive actuator design

The multibody dynamics model of the drag sail couples with the actuator equivalent force exerted on the system, which derives from the passive actuation of a shape memory alloy.

### 6.1. Configuration

The configuration of the SMA is the first key aspect to take into account in the design. Nitinol wires embedded in the origami structure are selected as actuators and they are aimed to exert a force capable of opening the creases angle. Two potential solutions are identified. The first concerns the use of axially shrinking wires embedded in the membrane, widely used in composite material. The wire lies perpendicular to the fold line and works both in traction and bending. However, it is subjected to highly concentrated stresses in the packed configuration, inducing localized plastic deformation and preventing complete deployment. This outcome, plus the low efficiency in the origami deployment, demonstrated experimentally (figure 4), leads to the discarding of this solution.

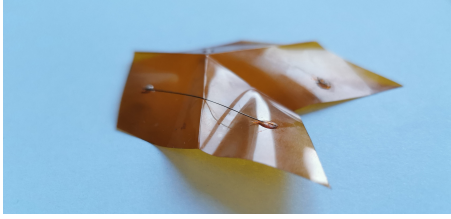


Figure 4: Experimental analysis: criticalities.

The above-stated issues are overcome by making use of the torsional wire configuration. The actuator lies along the crease line, limiting the size of the overall system and avoiding localized plastic deformations of the wire. The amount of recovered torsional strain depends on the length of the crease-aligned wire portion and can induce rotations greater than a full circle, ensuring the full deployment of the origami. The results of the actuation involving this kind of configuration are presented in the final section.

## 6.2. Torque exerted by the actuator

Once the wire configuration is chosen, the actuator design goes through the relationship between actuation force and wire temperature. The torque exerted by the wire is a function of the internal shear stress,  $T = \tau \frac{J}{r}$ , which in turn is determined by exploiting the constitutive model of the shape memory alloys [1].

$$\tau - \tau_0 = G(\gamma - \gamma_0) + \Omega(\xi_S - \xi_{S0}) + \Theta(T - T_0) \quad (6)$$

Equation 6 dictates the behavior of the actuator during the martensitic transformation. Starting from the martensite phase having an initial pre-strain  $\gamma_0$ , as the temperature rises above austenite start  $A_s$  the martensitic fraction  $\xi$  changes according to equation 7 and the wire starts recovering the strain.

$$\xi = \frac{\xi_0}{2} \left\{ \cos \left[ a_A \left( T - A_s - \frac{\sigma}{C_A} \right) \right] + 1 \right\} \quad (7)$$

Since the shape recovery is partially restrained by the stiffness of the origami, shear stress arises and the deployment is induced.

The temperature of the wire is computed with the aid of the heat transfer balance in equation 2, considering both the influence of the external environment, i.e. the radiation coming from the Sun and the Earth and the one leaving towards deep space, and the one of the drag sail membrane. As a matter of fact, the thin structure

both emits  $\dot{Q}_{\varepsilon,sail}$ , reflects  $\dot{Q}_{\rho,sail}$ , and conducts  $\dot{Q}_{cond,sail}$  heat, contributing to the overall energy balance of the wire. These terms are a function of the origami folding angle and thus depend on the self-view factor computed with the Monte Carlo method.

The torque computed with the aid of the constitutive relation is modeled in ADAMS as a concentrated torque located along the crease on which the SMA wire lies. Considering that the deployment angle trend is different for horizontal and vertical fold lines, the torque trend will be different too since it depends on the recovered strain. These two trend torques are computed in Simulink and fed to ADAMS.

## 7. Deployment simulation

The dynamic of the complete multibody model is carried out in a co-simulation involving Simulink and ADAMS. The choice of integrating MATLAB with ADAMS is dictated by the need to compute the torque from the constitutive model at each time step. Simulink is thus entrusted with solving the implicit equation in  $\tau$  and providing the solution to ADAMS.

### 7.1. Deployment optimization

The last step is identifying the optimal size and configuration of the wires. The two main design targets are the minimization of the packed volume and the maximization of the deployment. As regards the first aspect, the SMA wires are located just along the  $a$  since it guarantees the optimal configuration in terms of folded size. Future developments could be aimed at optimizing the wire design also from the point of view of the actuation force.

The maximization of the deployment is instead a matter of length, radius, and initial prestrain of the wires. These three parameters are strictly related to each other, influencing the recovered angle, the internal shear stress, and the deployment force. A long, thin wire can recover wide angles ( $\Delta\alpha = \frac{l}{r}\gamma_0$ ), but high shear stresses arise, overcoming the yield stress limit. On the contrary, short wires are not capable of recovering the completely unfolded configuration. Therefore, the optimization strategy consists of the minimization of the length and the maximization of the radius of the wire, by fixing a certain value of initial prestrain (figure 5).

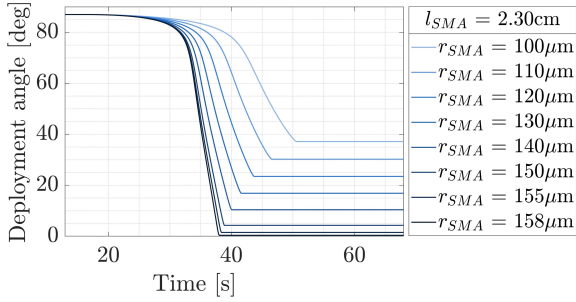


Figure 5: Convergence to the optimal solution.

## 7.2. Results

From the deployment optimization, it is obtained that to unfold a portion of the sail of  $2 \times 2$  cells a wire of dimensions equal to  $r = 158 \mu\text{m}$  and  $l = 2.3 \text{cm}$  is needed. This result does not scale with the dimension of the sail, but it just grows slightly as the number of cells increases: if, on the one hand, the larger the origami the higher the number of creases and thus the higher the rigidity of the system, on the other hand, as the number of wires increases the overall torque increases as well. The only parameter scaling with the dimension is the inertia of the sail, whose contribution is however almost negligible with respect to the rigidity of the creases.

The result is shown in figure 6, in which the trends of deployment angle and temperature over time are shown.

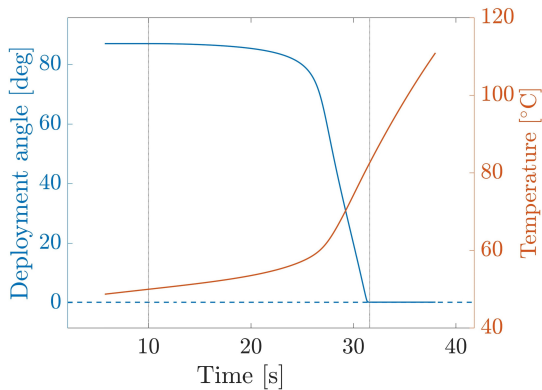


Figure 6: Simulink simulation scheme.

It is evident how the sail starts deploying as  $A_s$  is reached, while it stabilizes at  $\theta = 0^\circ$  at the end of the martensitic transformation. The effectiveness of the deployment is combined with interesting results in terms of volume and mass: considering a  $20 \times 11$  Miura-Ori origami equipped with wires of radius  $200 \mu\text{m}$  and length  $2.5 \text{cm}$  on each  $a$  crease, the packed width grows from

$4.8 \text{mm}$  up to about  $13 \text{mm}$ , perfectly compatible with the 1U stored dimension requirement, while the overall SMA actuators mass is about  $2 \text{g}$  ( $\sim 4.5 \text{mg}$  each).

The final analysis concerns the propagation of uncertainty on the SMA torque (equation 8). A 1% standard deviation on both radius and length produces a 3% variation in the generated torque, altering the deployment effectiveness.

$$\sigma_{T_w}^2 = \left( \frac{\partial T_w}{\partial r_w} \right)^2 \sigma_{r_w}^2 + \left( \frac{\partial T_w}{\partial l_w} \right)^2 \sigma_{l_w}^2 \quad (8)$$

## 8. Conclusions

The aim was to analyze the dynamics of the passive deployment of an origami drag sail. For this purpose, it was chosen to use SMA wires integrated into the origami structure as passive actuators, exploiting the one-way shape memory effect. The study's results show the system's effectiveness both in terms of dimensions and deployment. Although the increase in the volume of the sail is inevitable by adding the deployment system, the encumbrance and mass are much lower than in traditional deployment systems. Moreover, the autonomous deployment is not abrupt and immediate but gradual, reducing the risk of localized stress and sail breakage. Future developments could deepen the work by modeling the flexibility of the origami faces (FEM) and investigating the rigidization system of the fully deployed drag sail.

## References

- [1] L.C. Brinson. One-dimensional constitutive behavior of shape memory alloys: Thermomechanical derivation with non-constant material functions and redefined martensite internal variable. *Journal of Intelligent Material Systems and Structures*, 4(2):229–242, 1993.
- [2] Howard Curtis. *Orbital Mechanics For Engineering Students*. Butterworth-Heinemann, Boston, fourth edition edition, 2021.
- [3] M. Fossati. Origami engineering: Evaluation of patterns for deployable space structures. Master's thesis, Politecnico di Milano, 2022.
- [4] Hexagon AB. *Adams View Command User's Guide*, 2021.